THE JOURNAL OF PHYSICAL CHEMISTRY C

Article

pubs.acs.org/JPCC

Rapid Selective Etching of PMMA Residues from Transferred Graphene by Carbon Dioxide

Cheng Gong,[†] Herman Carlo Floresca,[†] David Hinojos,[†] Stephen McDonnell,[†] Xiaoye Qin,[†] Yufeng Hao,[‡] Srikar Jandhyala,[†] Greg Mordi,[†] Jiyoung Kim,[†] Luigi Colombo,[§] Rodney S. Ruoff,[‡] Moon J. Kim,[†] Kyeongjae Cho,[†] Robert M. Wallace,[†] and Yves J. Chabal*[,†]

[†]Department of Materials Science and Engineering, The University of Texas at Dallas, Richardson, Texas 75080, United States

[‡]Department of Mechanical Engineering and the Materials Science and Engineering Program, The University of Texas at Austin, Austin, Texas 78712, United States

[§]Texas Instruments Incorporated, Dallas, Texas 75243, United States

Supporting Information

ABSTRACT: During chemical-vapor-deposited graphene transfer onto target substrates, a polymer film coating is necessary to provide a mechanical support. However, the remaining polymer residues after organic solvent rinsing cannot be effectively removed by the empirical thermal annealing in vacuum or forming gas. Little progress has been achieved in the past years, for little is known about the chemical evolution of the polymer macromolecules and their interaction with the environment. Through in situ Raman and infrared spectroscopy studies of PMMA transferred graphene annealed in nitrogen, two main processes are uncovered involving the polymer dehydrogenation below 200 °C and a subsequent depolymerization above 200 °C. Polymeric carbons over the monolayer graphitic carbon are found to constitute a fundamental bottleneck for a thorough etching of PMMA residues. The dehydrogenated polymeric chains consist of active C═C bonding sites that are readily attacked by oxidative gases. The combination of Raman spectroscopy, X-ray photoemission spectroscopy, and transmission electron microscopy reveals the largely improved carbon removal by annealing in oxidative atmospheres. CO_2 outperforms other oxidative gases (e.g., NO_2, O_2) because of its moderate oxidative strength to remove polymeric carbons efficiently at 500 °C in a few minutes while preserving the underlying graphene lattice. The strategy and mechanism described here open the way for a significantly improved oxidative cleaning of transferred graphene sheets, which may require optimization tailored to specific applications.

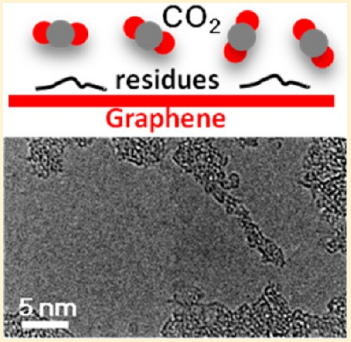

1. INTRODUCTION

Chemical vapor deposition (CVD) of methane on copper foil has constituted an economical way to obtain large-area high-quality monolayer graphene, compatible with conventional lithography for batch production of electronic devices, if there were a simple and effective process to transfer it onto the appropriate insulating substrates. With this goal in mind, a polymer-aided transfer has been developed and demonstrated.[1,2] A range of polymers, including poly(methyl methacrylate) (PMMA),[1] poly(bisphenol A carbonate) (PC),[3,4] polystyrene (PS),[5] thermal release tapes (TRT),[2,6] poly(dimethylsiloxane) (PDMS) stamps,[7,8] etc., have been utilized to aid the wet or dry transfer of graphene. Among the list of polymers, PMMA is widely used due to its availability, light transparency, ease of handling, variable viscosity, etc.[1−5,9−11] PMMA is also commonly used as a mask material for electron-beam lithography. While there have been recent efforts to develop a general method for transferring graphene onto any substrates, including soft materials,[12] polymer residues are still present and device fabrication also inevitably leaves e-beam resist residues, such as PMMA.

Unfortunately, the superior intrinsic properties of the transferred graphene ("Tr-Gr") are substantially degraded by the PMMA residues that also prevent high-resolution transmission electron microscopy (HRTEM) and scanning tunneling microscopy (STM) from probing the detailed atomic structure of Tr-Gr. Moreover, the doping profiles of graphene can be severely affected by charge transfer from/to the surface contaminants, leading to large variations of the electronic properties within a film, from film to film, and across different laboratories. The presence of such chemical contamination, therefore, greatly hinders the potential of this fascinating 2D material for surface-sensitive applications (e.g., biosensor,[13,14] DNA sequencing,[15] gas sensoring,[16−23] etc.) as well as the reproducibility of graphene-based high mobility field effect transistors (FETs). The fundamental understanding of the nature of the residues and their removal is critical to recover the intrinsic properties of Tr-Gr, stabilize the initial conditions of

Received: August 22, 2013
Revised: October 7, 2013
Published: October 10, 2013

   dx.doi.org/10.1021/jp408429v | J. Phys. Chem. C 2013, 117, 23000−23008

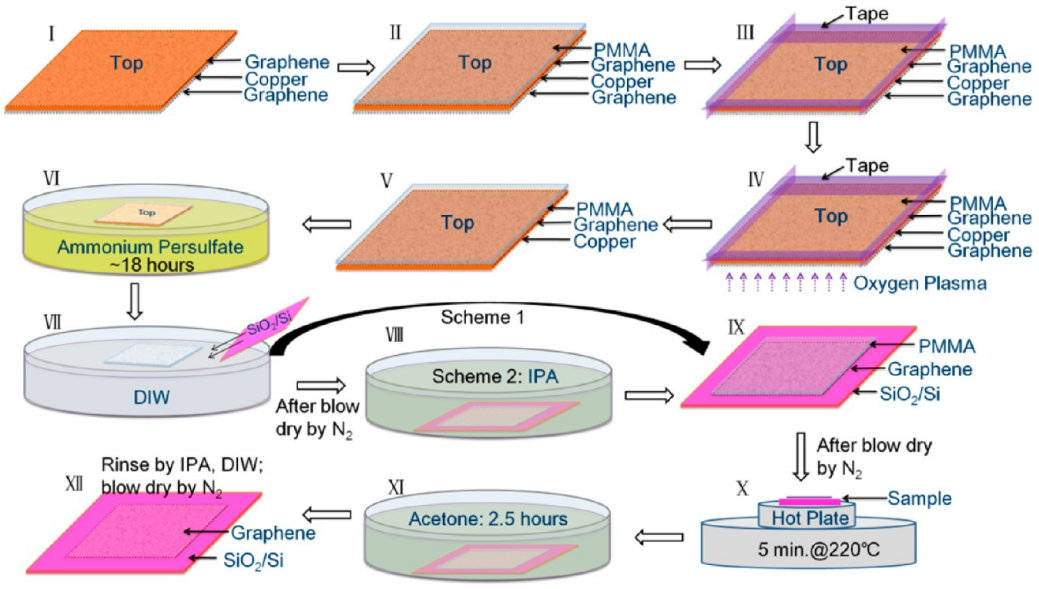

Figure 1. The process of PMMA-aided transferring of graphene from copper foil to SiO_2. Unless specified explicitly, all the samples in this work are prepared through "Scheme 2: IPA-aided transfer" at step VII–IX and are heated on the hot plate at 220 °C for 5 min in air at step X. After step XII, the sample is denoted as as-prepared Tr-Gr/SiO_2. DIW means deionized water.

Tr-Gr sheets, and standardize the performance of as-prepared devices for industrial applications of Tr-Gr.

Thermal annealing has been empirically applied to decompose and desorb PMMA residues. Much of the recent focus has been on the removal of oxygen-bearing species, probably due to the facts that (1) oxygen in the PMMA macromolecule is a foreign species that can covalently bond to graphene, and (2) oxygen as a charged impurity degrades the carrier mobility in graphene.[3,11,24] Intensive (many hours) annealing is commonly performed in vacuum[11,25,26] or reducing atmospheres,[4,26,27] leading to a drastic reduction of oxygen species, as evidenced by X-ray photoemission spectroscopy (XPS).[11,26] However, little is known about the fate of the remaining hydrocarbon backbones. In fact, TEM images show that the aforementioned extended thermal annealing still leaves a large amount of polymer-like residues, making it rather difficult to obtain large-area clean graphene patches even at the order of nanometers.[4] To address this issue, characterization of the chemical states of these postannealed residues and the conception of a new strategy for their improved removal are needed. We show here that these annealed residues are mostly carbons consisting of both sp^2 and sp^3 phases, and oxidative rather than reducing environments are best to remove them by attacking the sp^2-carbons. The effective removal of PMMA residues by annealing in CO_2 at 500 °C can be rapidly done, within a few minutes.

2. MATERIALS AND METHODS

2.1. Preparation of Transferred Graphene on SiO_2/Si Substrate. Large-area graphene films are grown by CVD of methane on Cu foils (Alfa Aesar, 99.8% purity) at 1035 °C in a halogen lamp-based quartz tube furnace.[1] The detailed transfer process is described in the flowchart of Figure 1. Since graphene grows on both sides of the Cu substrate, the graphene film grown on the bottom side is etched by reactive oxygen plasma (as shown in step III of Figure 1), to avoid a redeposition of broken graphene fragments from the bottom side onto the top graphene sheet during the solution-based Cu etching process. Isopropyl alcohol (IPA)-aided transfer was shown to promote the electrical performance of the as-prepared graphene transistors by driving water away from the graphene/SiO_2 interface.[28] Then, a brief (5 min) annealing at 220 °C on a hot plate is performed to minimize the wrinkles that are inevitably introduced during the mechanical transfer process and thereby smooth the contact between graphene and SiO_2. The substrates used in all the Raman and XPS studies are 85 nm SiO_2, thermally grown on highly p-doped silicon.

2.2. In Situ Raman Spectroscopic Study. In this work, the removal of the PMMA residues from Tr-Gr/SiO_2 is studied as a function of annealing temperatures (room temperature (RT) to 500 °C) in contrasting environments, including inert gas (N_2), reducing gases (forming gas (FG): 10%H_2/90%Ar, ethylene of 101.3 ppm in N_2), and oxidizing gases (CO_2 of purity 99.999%, extra dry grade O_2 of purity 99.8%, NO_2 of 1.005 mol % in N_2), in a reactor cell designed to fit a micro-Raman microscope stage for in situ measurements. Ultra-high-vacuum (UHV) annealing is done in a different chamber, and hence Raman spectroscopic study of the effect of UHV annealing is performed ex situ. Data are acquired by an Almega visible Raman spectrometer from Thermo Nicolet. All the gases are provided by Airgas.

The sample is loaded in a Linkam FTIR 600 cooling/heating stage connected with a continuous N_2 purge, which is readily switched to the other gases.[29] The 532 nm laser is focused onto the sample surface through a transparent quartz window located at the top of the Raman stage (abbreviated as "RS" hereafter). The sample is kept at the same position during the entire annealing and Raman characterization process, and selected gases are introduced into the RS without exposing the sample to the ambient. The target gas is introduced into the RS before annealing. The temperature ramp rate is 20 °C/min. After 30 min at the target temperature, N_2 is flowed through the RS as the temperature drops to 100 °C. This procedure helps remove gas molecules that would otherwise adsorb on the surface at lower temperatures. Once the temperature drops below 30 °C, 100 Raman spectra are collected over an area of

dx.doi.org/10.1021/jp408429v | J. Phys. Chem. C 2013, 117, 23000–23008

$20 \times 20\ \mu m^2$ with an interval of 2 μm (i.e., 10×10 data region sampling). Three methods are adopted to ensure the reliability of the data acquisition despite the nonuniformity of Tr-Gr caused by a random distribution of PMMA contaminants: (1) in situ experiments are done so that the laser scans the same area and the sample is never exposed to the air; (2) alignment marks are used for an accurate positioning before the start of each measurement, taking into account the possible microscale drifting of the sample during the thermal annealing process; and (3) mapping of an area of $20 \times 20\ \mu m^2$ is done to avoid nonrepresentative spots.

2.3. Ex Situ XPS and HRTEM Characterizations. XPS and HRTEM are complementary techniques for detecting the presence and subsequent removal of residual carbon species. HRTEM helps visualize any removal of surface impurities, and XPS is used to determine the elemental information of the removed contaminants. Both Tr-Gr/SiO_2 and suspended graphene samples are annealed in the RS and then loaded into the XPS and TEM chambers for characterization, respectively. The XPS analysis is carried out using a monochromatic Al Kα X-ray source, with an analyzer acceptance angle of 8°, a takeoff angle of 45°, and pass energy of 15 eV. HRTEM studies are performed, using a JEOL JEM-2100 transmission electron microscope, operating at 200 kV. Graphene films are transferred on silicon nitride substrates; each substrate has 16 prepatterned circular holes with a 5 μm diameter, thus forming regions of suspended graphene (see Figure S1 in the Supporting Information). To examine the same region of the graphene film in the systematic TEM measurements, a hole is created by the focused electron beam intentionally as a mark (see the Supporting Information). More than 10 TEM images are acquired in the regions nearby the reference hole in each measurement.

2.4. In Situ Fourier Transform Infrared Spectroscopy (FTIR) Study of the Thermal Behavior of PMMA Residues. The substrates used in the FTIR studies are double-sided polished low-doped FZ (50 Ohm·cm) Si(100) wafers with a 7 nm thick thermal oxide (SiO_2). Graphene sheets are transferred on both sides of the substrate to double the IR absorption in a transmission-mode geometry. The detailed mechanical and chemical cleaning of the Si wafer surface was described in our previous work.[30] The substrate surface is carefully cleansed to minimize interface contaminants that could severely influence both optical and photoelectronic measurements. Considering that the behaviors of residual carbons are the focus of this work, clean surfaces free of organic contaminants are crucial. The FTIR spectrometer is a Nicolet 6700 from Thermo Scientific. The single-beam FTIR spectra are acquired at 60 °C after 30 min annealing at target temperatures. All the thermal annealing and FTIR data acquisition is carried out in situ in a vacuum chamber of 10^{-3} Torr.

3. RESULTS AND DISCUSSION

3.1. Thermal Behavior of PMMA Residues in Inert Environments. Since UHV conditions cannot be obtained in the RS, N_2 purge gas is used. Raman spectroscopy is then used to determine whether the N_2 environment affects the sample. Figure 2a shows that the broad contributions within the 1050–1550 cm^{-1} region to the Raman spectra of Tr-Gr/SiO_2 samples annealed in N_2, UHV ($P = 10^{-9}$ Torr), and FG at 500 °C for 30 min, are similar for these conditions. A tiny shift of the G peak is not relevant here and will be discussed in another paper. The

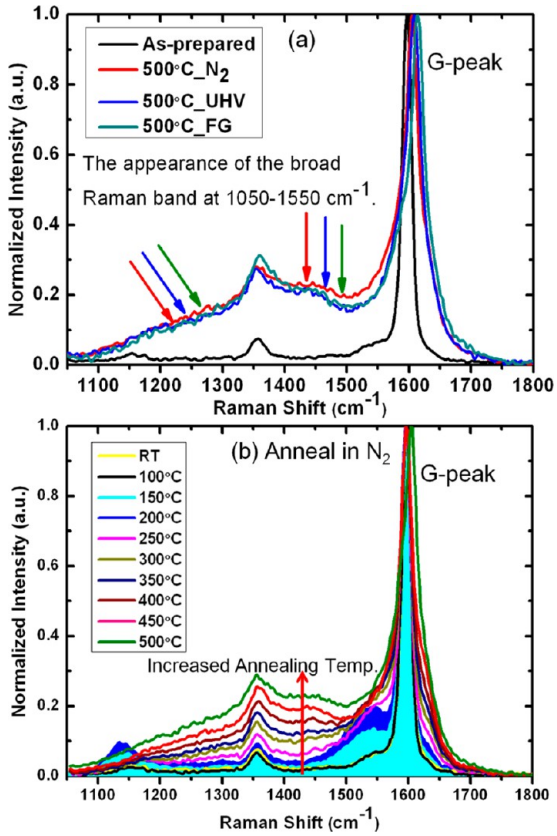

Figure 2. (a) The comparison of Raman spectra of the Tr-Gr/SiO_2 after being annealed at 500 °C in N_2, UHV, and FG; the parallel arrows in red, blue, and green colors point to the annealing induced broad Raman band. (b) Raman spectra of the Tr-Gr/SiO_2 after N_2 annealing at different temperatures. In both figures, the G peak intensities of all spectra are normalized. Raman data are always acquired at RT in N_2.

focus of the present work is on the broad band (1050–1550 cm^{-1}) that is the fingerprint of residual carbons, as discussed in the rest of this paper.

The evolution of this broad band is summarized in Figure 2b, which shows the Raman results of Tr-Gr/SiO_2 as a function of annealing temperatures from RT (yellow) to 500 °C (green) in N_2. There are two notable behaviors in these spectra, compared to the starting spectrum (the yellow curve for as-prepared sample): First, after 150 and 200 °C annealing, two new Raman peaks appear, centered at ~1133 and ~1523 cm^{-1}. These two well-defined peaks are presumably associated with an ordered structure because they are relatively sharp compared to the broad band. They both have the same dependence on thermal annealing: appearing upon 150 °C, increasing upon 200 °C, and broadening above 200 °C annealing temperature. Second, the intensity of the broad Raman band increases monotonically with the annealing temperature above 200 °C.

The appearance of the new Raman peaks is common to samples prepared with slightly modified conditions as well. For instance, samples heated on a hot plate at only 180 °C (instead of 220 °C as shown in step X of Figure 1) still exhibit the two new Raman peaks (more intense in this case), confirming their existence, as shown in Figure S3 (Supporting Information). Their high intensity makes it possible to confirm that they have exactly the same behavior (a simultaneous intensity decrease) upon controlled heating by the focused Raman laser. In

dx.doi.org/10.1021/jp408429v | J. Phys. Chem. C 2013, 117, 23000–23008

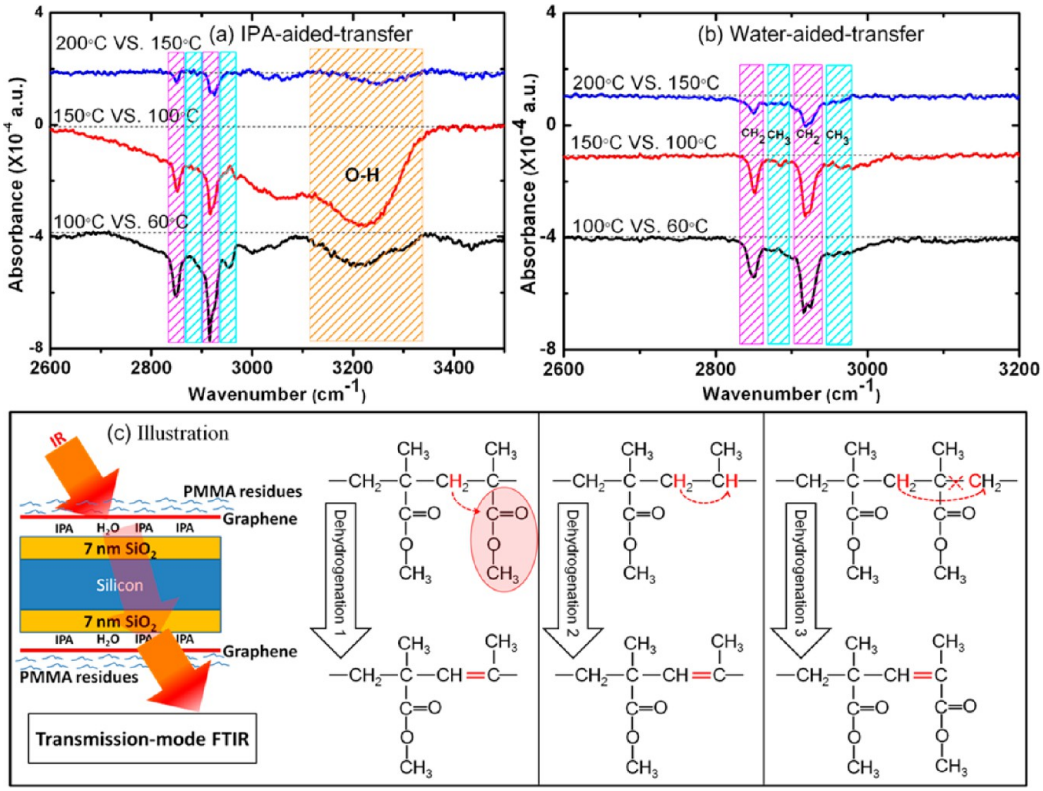

Figure 3. FTIR differential spectra of the (a) IPA-aided and (b) water-aided double-sided Tr-Gr/SiO_2. Panel (c) shows the illustration of the transmission-mode FTIR measurement of the double-sided Tr-Gr/SiO_2 sample by IPA-aided transfer. Possible dehydrogenation pathways of PMMA residues are illustrated in (c). The sample illustration in (c) is not to scale.

summary, there are two transient features obtained upon 150–200 °C annealing, then broadening to contribute to the broad band. Their origin is discussed next.

3.2. Origin of the New Raman Peaks: Dehydrogenated PMMA Residues. The higher frequency peak, at $\nu \sim 1523$ cm^{-1}, is characteristic of the stretching modes of a polyenic chain.[31] Previous Raman spectroscopic studies of the diamond-like carbon (DLC) have documented the dependence of the Raman G peak position on the composition ratio between sp^2- and sp^3-carbons. Depending on the ratio of sp^2- and sp^3-carbons in the DLC, the G peak position was shown to vary in the range of ~1510–1600 cm^{-1}.[32] Moreover, Ferrari et al. have confirmed that the Raman peak at ~1150 cm^{-1} (i.e., corresponding to our lower-frequency peak) observed in CVD diamond cannot originate from a nanodiamond or related sp^3-bonded phase, but must arise from coexisting sp^2-carbons, which is thought to be due to *trans*-polyacetylene segments in the grain boundaries and surfaces.[33] These studies suggest that our two new Raman peaks arise from polyenic chains. This conclusion is further supported by another study of *trans*-polyacetylene,[34] wherein both Raman peaks at 1126 and 1526 cm^{-1} were observed under laser irradiation of 457.9 nm. All these studies collectively agree with the assignment of the observed two new Raman peaks to sp^2-carbons in polymeric structures. In the Tr-Gr/SiO_2 samples, PMMA residues and their derivatives are the only polymeric structures that can contribute to the Raman peaks at ~1133 and 1523 cm^{-1}.[4]

Note that the appearance of the new Raman peaks and the broad band upon annealing does not mean an increased contamination; however, it is a result of a chemical state transformation of PMMA residues from sp^3- to sp^2-carbons. The relative increase in intensity arises from the fact that the cross section of the sp^2-carbon in Raman scattering with 514.5 nm excitation (close to the 532 nm used in this work) is 50–200 times stronger than that of sp^3-carbon.[32] Therefore, most residual carbons that are in an sp^3-bonding configuration in as-prepared Tr-Gr samples cannot contribute to the Raman spectrum, and only after they are transformed to sp^2-carbons can the Raman cross section be large enough to be detected.

The origin of this transformation is best studied using infrared absorption studies. For instance, if thermo-activated dehydrogenation of residual PMMA macromolecules takes place (necessary for sp^3- to sp^2-carbon transformation), then the loss of hydrogen should be detectable with in situ FTIR during annealing. For FTIR study, either DIW or IPA solvent is used to transfer graphene on SiO_2. The use of IPA was motivated by our observation that the graphene transferred by IPA has fewer broken areas and higher mobility than that by DIW because trapped water is believed to induce scattering.[28] For the specific purpose in this work, IPA and DIW provide samples with different interface chemistry, which can be used to help identify the common features as from surface residues and the different features as from the interface. Figure 3a,b clearly shows that, upon below 200 °C annealing, both samples have the same decomposition behavior in the CH_2 stretching region, related to surface residues. The difference in the red curves of Figure 3a,b (i.e., the strong and broad OH stretching band) is caused by the intercalated IPA at graphene/SiO_2 interfaces. As illustrated in Figure 3c, the PMMA molecular formula shows that CH_2 forms the backbone of PMMA polymer chains, and CH_3 is a ligand. The large amount of CH_2 decomposition, therefore, suggests that the sp^3-carbons in polymer backbones

dx.doi.org/10.1021/jp408429v | J. Phys. Chem. C 2013, 117, 23000–23008

are dehydrogenated. Although the specific dehydrogenation pathways may vary due to the variety of the local atomic arrangements within residues (see Figure 3c), the overall result is an increased population of sp^2-carbons.

When annealing over 200 °C, the residual chains are depolymerized into segments of varying lengths. Due to the different environments of sp^2-carbons and the varying polymer lengths, Raman peaks broaden spanning the 1050−1550 cm^{-1} range. Indeed, Ferrari et al. have shown that the formation of different length segments of conjugated carbons leads to a broadening of these Raman modes.[33]

3.3. Oxidative Etching of the Dehydrogenated PMMA Residues: Raman and IR Evidence. Comparative studies have been performed to determine the principal factor for PMMA residue removal based on 500 °C annealing in contrasting atmospheres: reducing gases (FG and C_2H_4) and oxidative gases (O_2, CO_2, and NO_2). For safety considerations, C_2H_4 is diluted in N_2 (101.3 ppm) at atmospheric pressure, equivalent to a pressure of 0.077 Torr of pure ethylene. The choice of C_2H_4 instead of saturated hydrocarbons (e.g., alkanes) is based on its simplicity (smallest alkene) and its higher reactivity due to its C═C double bond. NO_2, as a toxic gas, is balanced by N_2 at 1.005 mol %. The oxidative strengths follow the sequence CO_2 < O_2 < NO_2, with various bond strengths (C═O in CO_2: ~532 kJ/mol^{-1}; O═O in O_2: ~497 kJ/mol^{-1}; N−O in NO_2: ~306 kJ/mol^{-1}).[35]

Two main findings are obtained from the Raman results in Figure 4a. First, in contrast to FG and C_2H_4, treatments in all of the three oxidative gases examined here effectively eliminate the broad Raman band that is associated with residual carbons. Second, NO_2 etches away the graphene film, O_2 destructs the graphene lattice with notable D-peak formation, while CO_2 preserves the graphene with a similar D-peak intensity to the as-prepared sample.

We infer that the presence of C═C bonds provides active sites for oxidative gases to attack and decompose the polymer chains, facilitating the improved removal of PMMA residues. This is the well-known aging mechanism of many types of elastomers, wherein traces of ozone in air attack the double bonds in rubber chains.[36] As shown in Figure 4c, after 1 h annealing at 500 °C in vacuum, an additional 1 h of annealing of the same sample at 500 °C in CO_2 shows a further removal of sp^2-carbons, indicating the attack of C═C bonding sites of polymer residues by CO_2. Since C═C bonding is IR-inactive in pristine graphene but activated by defects, the loss of the C═C stretching mode detected in the IR absorption spectrum can only be a result of the removal of PMMA residues.

In line with the oxidative strength relationship CO_2 < O_2 < NO_2, oxidative etching plays a significant role on both PMMA residues and graphene. It is consistent with a previous work showing that oxygen partially etches graphite at 500 °C.[37] These experimental observations suggest that less aggressive oxidative gases are desirable for maintaining the quality of pristine graphene. Although there are sp^2-carbons in both dehydrogenated PMMA residues and graphene, PMMA residues constitute a type of defect that is more reactive than the pristine graphene. Selective etching of the surface residues over underlying graphene film can be realized but needs particular caution at determining environments and annealing temperatures.

The strongest oxidative gas among the three, NO_2, completely etches all of the single-layer graphene film, leaving some adlayer regions (see inset in Figure 4). The presence of

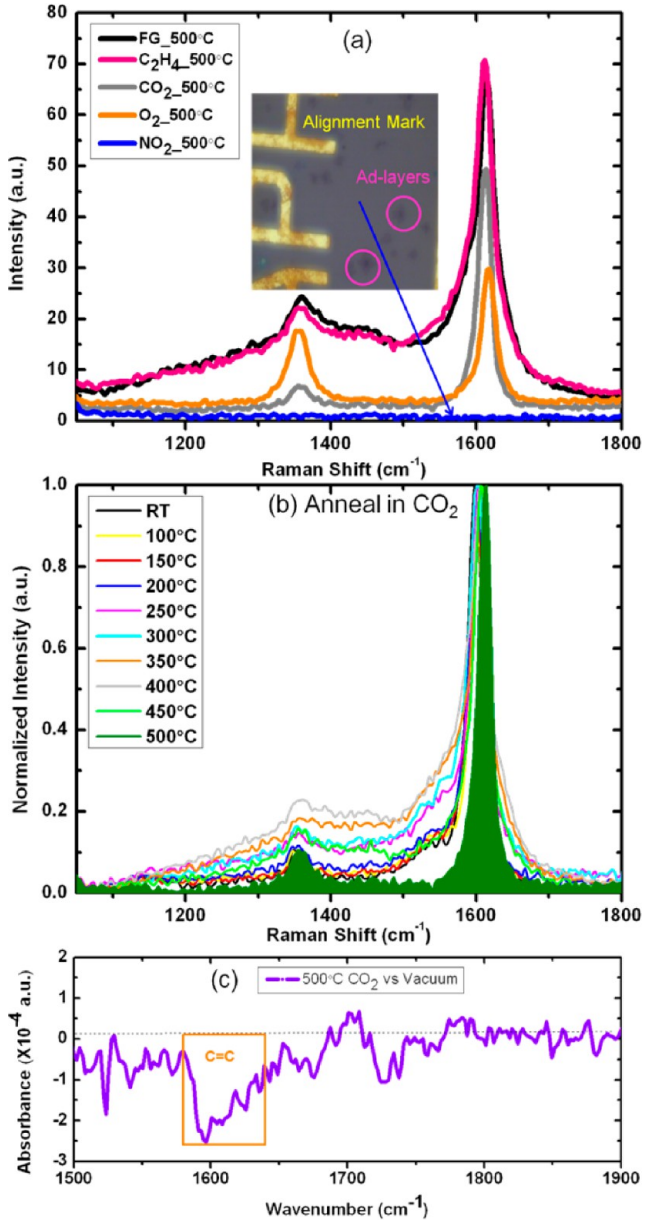

Figure 4. (a) Raman spectra of the Tr-Gr/SiO_2 after 30 min 500 °C annealing in various gases. (b) Annealing temperature dependence of Raman spectra of the Tr-Gr/SiO_2 in CO_2. The inset optical image of (a) shows Tr-Gr/SiO_2 after 30 min 500 °C annealing in NO_2. Panel (c) is an FTIR differential spectrum of a Tr-Gr/SiO_2/Si/SiO_2/Tr-Gr sample annealed at 500 °C in vacuum for 1 h, followed by another 1 h annealing at 500 °C in CO_2.

adlayers after etching indicates that the process is dependent on the initial graphene thickness (number of graphene layers). Such selective etching has already been reported with O_2.[37] Monolayer graphene is deformed by intimate contact with the atomically rough SiO_2 substrate, thus fostering reactivity and etching of graphene by reactive gases. In contrast, top layers of multilayer graphene films are decoupled from the rough substrates. Therefore, oxidative etching of monolayer graphene is easier than that of multilayer graphene, and oxidative etching of supported graphene is easier than that of suspended graphene. This explains why the TEM images of suspended graphene in Figure 6 barely show visible degradation after 30 min 500 °C annealing in O_2, yet defect formation for Tr-Gr/

dx.doi.org/10.1021/jp408429v | J. Phys. Chem. C 2013, 117, 23000−23008

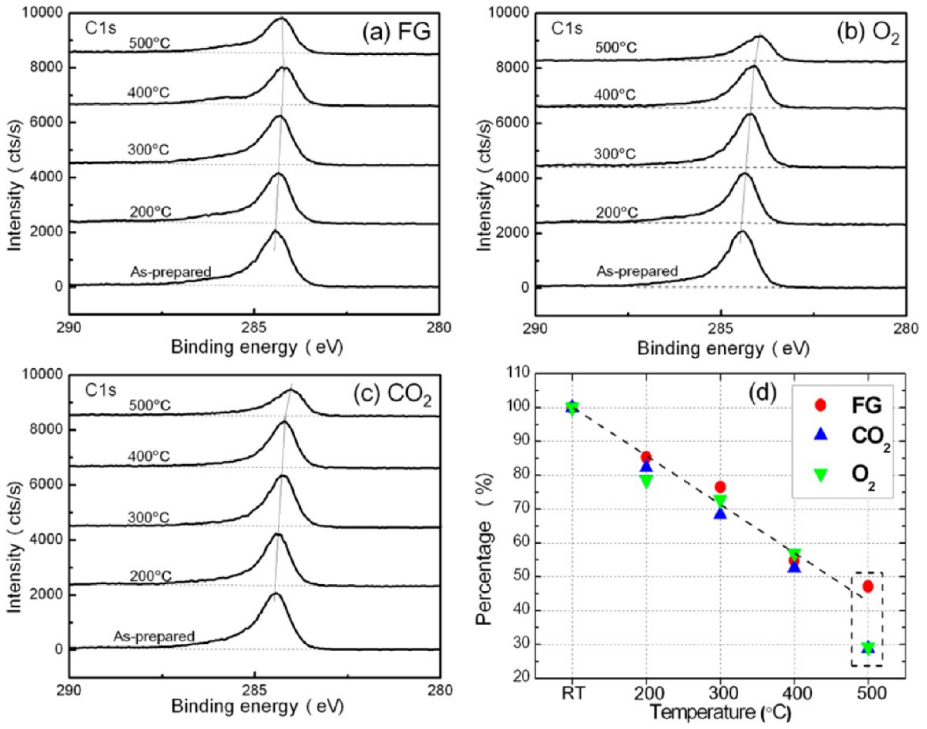

Figure 5. C 1s XPS spectra of the Tr-Gr/SiO_2 after annealing at systematic temperatures in (a) FG, (b) O_2, and (c) CO_2. Panel (d) is the summary of the percentage change of the integrated areas of XPS C 1s peaks of the Tr-Gr/SiO_2 after a series of annealing, normalized to that of the as-prepared samples.

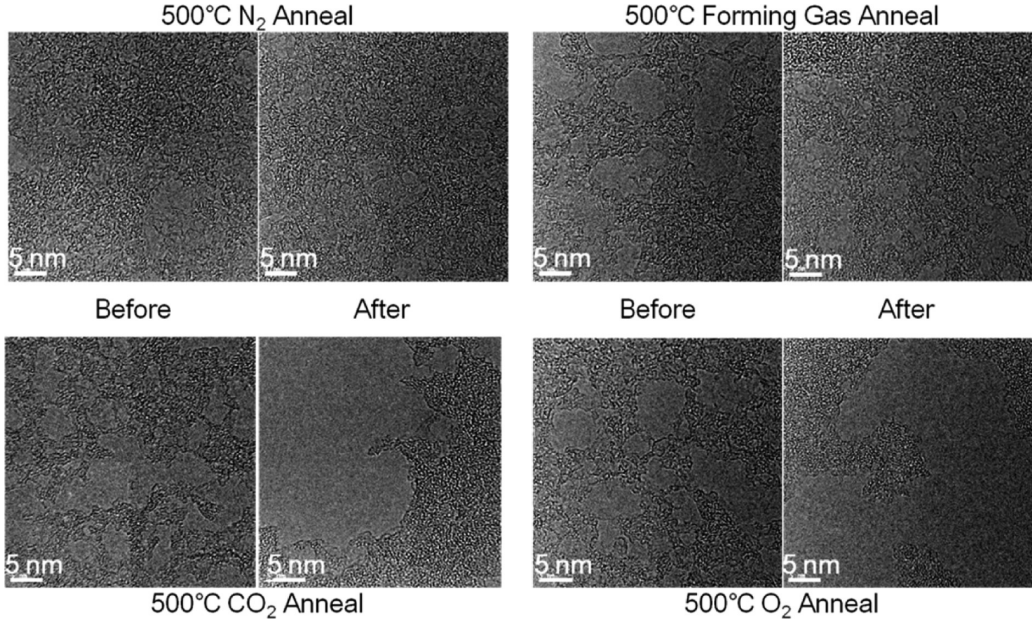

Figure 6. Representative HRTEM images of the transferred suspended graphene before and after 500 °C annealing in various atmospheres.

SiO_2 subjected to the same annealing process is clear, as evidenced by a strong Raman D-peak.

3.4. XPS Evidence of Highly-Efficient Removal of Residual Carbons. To determine that the removed residues during the gas treatment mainly consist of carbon species and to quantify such removal (carbon, in particular), XPS measurements are performed. The XPS data are normalized to the integrated area of the Si 2p peak for calculating the percentage loss of carbon species. In Figure 5, a decrease of the integrated C 1s peak area is observed as a function of annealing temperature. Upon low-temperature annealing, there is little difference among treatments in FG, O_2, and CO_2. However, after 500 °C annealing, the C 1s intensities decrease to 47.2% in FG, 28.8% in O_2, and 29.2% in CO_2.

The sensitivity to defects is different for XPS and Raman. While the presence of a few point defects causes a noticeable increase of the Raman D-peak intensity, the same density of defects is undetectable in XPS. Moreover, the exact location probed in XPS scans (~0.4 mm spot size) cannot be as precisely controlled as it is in Raman (~0.7 μm spot size). It is,

dx.doi.org/10.1021/jp408429v | J. Phys. Chem. C 2013, 117, 23000−23008

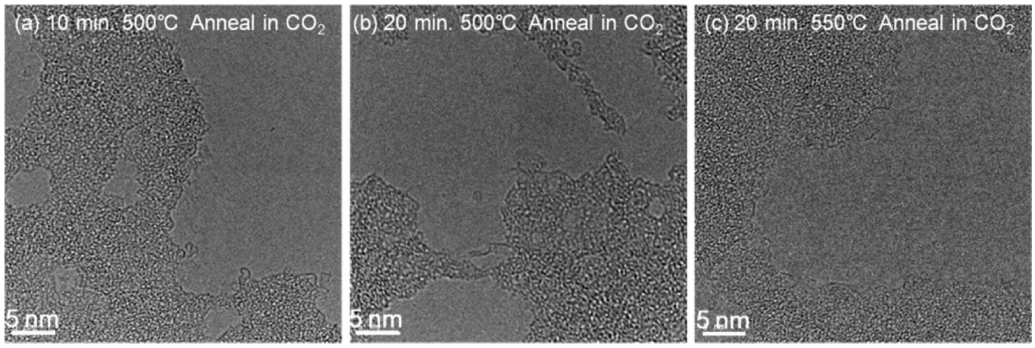

Figure 7. Representative HRTEM images of the transferred suspended graphene after (a) 10 min 500 °C annealing, (b) 20 min 500 °C annealing, and (c) 20 min 550 °C annealing in CO_2, respectively. These three images are from the same sample after sequential annealing: i.e., (a) 10 min at 500 °C, (b) a second 10 min at 500 °C, and (c) another 20 min at 550 °C.

therefore, reasonable that XPS results do not show visible differences between samples etched in CO_2 and O_2, but Raman results do.

The procedure for the removal of PMMA residues commonly used in many laboratories is "annealing in FG at 300 °C", which only reduces the C 1s intensity to 76.5% of its initial value, according to our quantitative XPS analysis. In contrast, annealing in FG and CO_2 at 500 °C leads to approximately twice and 3 times the removal of residual carbons. This leads to a surprising conclusion that, after the standard cleaning procedure in FG at 300 °C, a majority of the detected carbons by XPS are from PMMA residues instead of graphene. Removing these residual carbons from the underlying graphitic carbons constitutes a fundamental bottleneck for a thorough cleaning of Tr-Gr.

In all cases shown in Figure 5a–c, there is a shift of the C 1s core-level peak to lower binding energies after high-temperature annealing. This indicates an increased p-type doping of graphene, because the measured core-level electron binding energy is reduced with respect to the Fermi level. Such p-type doping is also supported by a blue shift of the G peak in the Raman spectra and the correspondingly decreased intensity ratio of 2D peak and G peak. The doping behavior of Tr-Gr upon thermal cleaning is interesting and complex and will be discussed in a forthcoming paper. Briefly, the increased p-type doping of graphene is a combined result of a closer contact with the SiO_2 substrate, interface chemistry evolution, and a decomposition of PMMA residues, but not a result of graphene oxidation by the oxidative gases.

3.5. Imaging the Postannealed Transferred Graphene: Evaluation of the Environments, Annealing Temperatures, and Durations. HRTEM studies are performed to directly assess the cleanness of graphene. Images in Figure 6 show large variations of the as-prepared graphene sheets, due to a random distribution of surface contaminants. As claimed before, these variations are detrimental for the precise control of the graphene quality and uniformity. The HRTEM data show that annealing in FG and N_2 gives similar results (very limited cleaning at 500 °C), and annealing in CO_2 as well as that in O_2 shows improved removal of PMMA residues at 500 °C. These conclusions are consistent with previous Raman and XPS characterization. Since suspended graphene is used, there is no discernible evidence that graphene is damaged by O_2 annealing at 500 °C.

Figure 7a,b shows that the TEM images of the Tr-Gr sample after 10 and 20 min annealing at 500 °C in CO_2 do not exhibit notable differences, suggesting a rapid cleaning process in a few minutes. Increasing the annealing temperature to 550 °C (see Figure 7c) does not affect the TEM results for *suspended* graphene, but induces an increased intensity of defects, as seen in an increase of Raman D-peak intensity for *supported* graphene (not shown here). Therefore, for supported graphene on SiO_2, CO_2 annealing at temperatures above 500 °C does not help the removal of PMMA residues much, but instead damages the graphene lattice substantially.

In closing, we stress that this work has focused on the chemical and structural effects of PMMA residues cleaning. The investigation of the electronic transport properties of the postannealed graphene by electrical characterization is in progress to derive a comprehensive evaluation of its potential applications in electronic devices.

4. CONCLUSIONS

In conclusion, a systematic in situ Raman study of transferred graphene on SiO_2/Si as a function of annealing temperature shows that residual PMMA macromolecules dehydrogenate into polyenic chains with a mixture of sp^2- and sp^3-carbons upon 150–200 °C annealing, exhibiting two new Raman peaks at ~1133 and ~1523 cm^{-1}. Annealing above 200 °C decomposes the chains into fragments of varying lengths, leading to a broad Raman band in the 1050–1550 cm^{-1} region. Oxidative ambients (CO_2, O_2, and NO_2) are shown to be more effective in removing these carbon fragments than reducing ambients (e.g., forming gas) or vacuum by attacking the C=C bonding sites in dehydrogenated PMMA residues. However, careful consideration of the oxidative strengths of the ambient gases and the annealing temperatures is critical for achieving the selective etching of the organic residues without damaging the underlying graphene film.

The present systematic study suggests that annealing in atmospheric CO_2 at 500 °C in a few minutes is effective in removing PMMA (i.e., mainly carbon) residues with negligible damage to the transferred graphene sheet on a SiO_2 substrate. The effectiveness in removing carbon residues is important for any transfer or processing method involving polymers, such as patterning, because the thermal cleaning invariably leaves residual carbons. CO_2 is, therefore, recommended as an appropriate environmental gas for improved thermal cleaning of the transferred graphene, due to its medium oxidizing reactivity, nontoxicity, absence of impurity species, low cost, and easy application without increasing experimental complexity. The mechanism uncovered in this specific PMMA/graphene system has a broad impact on a generic system

dx.doi.org/10.1021/jp408429v | J. Phys. Chem. C 2013, 117, 23000–23008

where organic contaminants need to be delicately removed from carbon nanomaterial as a host template.

■ ASSOCIATED CONTENT

Supporting Information

The SEM image of suspended graphene on prepatterned holes, the reference hole for TEM imaging, and Raman spectra of the sample prepared by a slightly modified condition for confirming the existence and the same origin of the two new Raman peaks. This material is available free of charge via the Internet at http://pubs.acs.org.

■ AUTHOR INFORMATION

Corresponding Author

*E-mail: chabal@utdallas.edu. Phone: +1 (972)-883-5751. Fax: +1 (972)-883-5725.

Notes

The authors declare no competing financial interest.

■ ACKNOWLEDGMENTS

This work was supported partly by NSF (CHE-0911197), AOARD-AFOSR (FA2385-10-1-4066), and the NRI SWAN Center.

■ REFERENCES

(1) Li, X. S.; Cai, W. W.; An, J. H.; Kim, S.; Nah, J.; Yang, D. X.; Piner, R.; Velamakanni, A.; Jung, I.; Tutuc, E.; et al. Large-Area Synthesis of High-Quality and Uniform Graphene Films on Copper Foils. *Science* **2009**, *324*, 1312−1314.

(2) Bae, S.; Kim, H.; Lee, Y.; Xu, X. F.; Park, J. S.; Zheng, Y.; Balakrishnan, J.; Lei, T.; Kim, H. R.; Song, Y. I.; et al. Roll-to-Roll Production of 30-in. Graphene Films for Transparent Electrodes. *Nat. Nanotechnol.* **2010**, *5*, 574−578.

(3) Park, H. J.; Meyer, J.; Roth, S.; Skakalova, V. Growth and Properties of Few-layer Graphene Prepared by Chemical Vapor Deposition. *Carbon* **2010**, *48*, 1088−1094.

(4) Lin, Y. C.; Jin, C. H.; Lee, J. C.; Jen, S. F.; Suenaga, K.; Chiu, P. W. Clean Transfer of Graphene for Isolation and Suspension. *ACS Nano* **2011**, *5*, 2362−2368.

(5) Lock, E. H.; Baraket, M.; Laskoski, M.; Mulvaney, S. P.; Lee, W. K.; Sheehan, P. E.; Hines, D. R.; Robinson, J. T.; Tosado, J.; Fuhrer, M. S.; et al. High-Quality Uniform Dry Transfer of Graphene to Polymers. *Nano Lett.* **2012**, *12*, 102−107.

(6) Caldwell, J. D.; Anderson, T. J.; Culbertson, J. C.; Jernigan, G. G.; Hobart, K. D.; Kub, F. J.; Tadjer, M. J.; Tedesco, J. L.; Hite, J. K.; Mastro, M. A.; et al. Technique for the Dry Transfer of Epitaxial Graphene onto Arbitrary Substrates. *ACS Nano* **2010**, *4*, 1108−1114.

(7) Kim, K. S.; Zhao, Y.; Jang, H.; Lee, S. Y.; Kim, J. M.; Kim, K. S.; Ahn, J. H.; Kim, P.; Choi, J. Y.; Hong, B. H. Large-Scale Pattern Growth of Graphene Films for Stretchable Transparent Electrodes. *Nature* **2009**, *457*, 706−710.

(8) Mattevi, C.; Kim, H.; Chhowalla, M. A Review of Chemical Vapour Deposition of Graphene on Copper. *J. Mater. Chem.* **2011**, *21*, 3324−3334.

(9) Shi, Y. M.; Kim, K. K.; Reina, A.; Hofmann, M.; Li, L. J.; Kong, J. Work Function Engineering of Graphene Electrode via Chemical Doping. *ACS Nano* **2010**, *4*, 2689−2694.

(10) Yu, Q. K.; Jauregui, L. A.; Wu, W.; Colby, R.; Tian, J. F.; Su, Z. H.; Cao, H. L.; Liu, Z. H.; Pandey, D.; Wei, D. G.; et al. Control and Characterization of Individual Grains and Grain Boundaries in Graphene Grown by Chemical Vapour Deposition. *Nat. Mater.* **2011**, *10*, 443−449.

(11) Pirkle, A.; Chan, J.; Venugopal, A.; Hinojos, D.; Magnuson, C. W.; McDonnell, S.; Colombo, L.; Vogel, E. M.; Ruoff, R. S.; Wallace, R. M. The Effect of Chemical Residues on the Physical and Electrical Properties of Chemical Vapor Deposited Graphene Transferred to SiO_2. *Appl. Phys. Lett.* **2011**, *99*, 122108.

(12) Song, J.; Kam, F. Y.; Png, R. Q.; Seah, W. L.; Zhuo, J. M.; Lim, G. K.; Ho, P. K. H.; Chua, L. L. A General Method for Transferring Graphene onto Soft Surfaces. *Nat. Nanotechnol.* **2013**, *8*, 356−362.

(13) Dong, X. C.; Shi, Y. M.; Huang, W.; Chen, P.; Li, L. J. Electrical Detection of DNA Hybridization with Single-Base Specificity Using Transistors Based on CVD-Grown Graphene Sheets. *Adv. Mater.* **2010**, *22*, 1649−1653.

(14) Hess, L. H.; Jansen, M.; Maybeck, V.; Hauf, M. V.; Seifert, M.; Stutzmann, M.; Sharp, I. D.; Offenhausser, A.; Garrido, J. A. Graphene Transistor Arrays for Recording Action Potentials from Electrogenic Cells. *Adv. Mater.* **2011**, *23*, 5045−5049.

(15) Min, S. K.; Kim, W. Y.; Cho, Y.; Kim, K. S. Fast DNA Sequencing with a Graphene-Based Nanochannel Device. *Nat. Nanotechnol.* **2011**, *6*, 162−165.

(16) Schedin, F.; Geim, A. K.; Morozov, S. V.; Hill, E. W.; Blake, P.; Katsnelson, M. I.; Novoselov, K. S. Detection of Individual Gas Molecules Adsorbed on Graphene. *Nat. Mater.* **2007**, *6*, 652−655.

(17) Wehling, T. O.; Novoselov, K. S.; Morozov, S. V.; Vdovin, E. E.; Katsnelson, M. I.; Geim, A. K.; Lichtenstein, A. I. Molecular Doping of Graphene. *Nano Lett.* **2008**, *8*, 173−177.

(18) Dan, Y. P.; Lu, Y.; Kybert, N. J.; Luo, Z. T.; Johnson, A. T. C. Intrinsic Response of Graphene Vapor Sensors. *Nano Lett.* **2009**, *9*, 1472−1475.

(19) Kong, J.; Franklin, N. R.; Zhou, C. W.; Chapline, M. G.; Peng, S.; Cho, K. J.; Dai, H. J. Nanotube Molecular Wires as Chemical Sensors. *Science* **2000**, *287*, 622−625.

(20) Yavari, F.; Castillo, E.; Gullapalli, H.; Ajayan, P. M.; Koratkar, N. High Sensitivity Detection of NO_2 and NH_3 in Air Using Chemical Vapor Deposition Grown Graphene. *Appl. Phys. Lett.* **2012**, *100*, 203120.

(21) Crowther, A. C.; Ghassaei, A.; Jung, N.; Brus, L. E. Strong Charge-Transfer Doping of 1 to 10 Layer Graphene by NO_2. *ACS Nano* **2012**, *6*, 1865−1875.

(22) Ren, Y. J.; Zhu, C. F.; Cai, W. W.; Li, H. F.; Ji, H. X.; Kholmanov, I.; Wu, Y. P.; Piner, R. D.; Ruoff, R. S. Detection of Sulfur Dioxide Gas with Graphene Field Effect Transistor. *Appl. Phys. Lett.* **2012**, *100*, 163114.

(23) Romero, H. E.; Joshi, P.; Gupta, A. K.; Gutierrez, H. R.; Cole, M. W.; Tadigadapa, S. A.; Eklund, P. C. Adsorption of Ammonia on Graphene. *Nanotechnology* **2009**, *20*, 245501.

(24) Ahn, Y.; Kim, H.; Kim, Y.-H.; Yi, Y.; Kim, S.-I. Procedure of Removing Polymer Residues and Its Influences on Electronic and Structural Characteristics of Graphene. *Appl. Phys. Lett.* **2013**, *102*, 091602.

(25) Romero, H. E.; Shen, N.; Joshi, P.; Gutierrez, H. R.; Tadigadapa, S. A.; Sofo, J. O.; Eklund, P. C. n-Type Behavior of Graphene Supported on Si/SiO_2 Substrates. *ACS Nano* **2008**, *2*, 2037−2044.

(26) Lin, Y. C.; Lu, C. C.; Yeh, C. H.; Jin, C. H.; Suenaga, K.; Chiu, P. W. Graphene Annealing: How Clean Can It Be? *Nano Lett.* **2012**, *12*, 414−419.

(27) Ratinac, K. R.; Yang, W. R.; Ringer, S. P.; Braet, F. Toward Ubiquitous Environmental Gas Sensors—Capitalizing on the Promise of Graphene. *Environ. Sci. Technol.* **2010**, *44*, 1167−1176.

(28) Chan, J.; Venugopal, A.; Pirkle, A.; McDonnell, S.; Hinojos, D.; Magnuson, C. W.; Ruoff, R. S.; Colombo, L.; Wallace, R. M.; Vogel, E. M. Reducing Extrinsic Performance-Limiting Factors in Graphene Grown by Chemical Vapor Deposition. *ACS Nano* **2012**, *6*, 3224−3229.

(29) Gong, C.; Hinojos, D.; Wang, W. C.; Nijem, N.; Shan, B.; Wallace, R. M.; Cho, K. J.; Chabal, Y. J. Metal−Graphene−Metal Sandwich Contacts for Enhanced Interface Bonding and Work Function Control. *ACS Nano* **2012**, *6*, 5381−5387.

(30) Gong, C.; Acik, M.; Abolfath, R. M.; Chabal, Y.; Cho, K. Graphitization of Graphene Oxide with Ethanol during Thermal Reduction. *J. Phys. Chem. C* **2012**, *116*, 9969−9979.

(31) Turrell, G., Corset, J., Eds. *Raman Microscopy: Developments and Applications*; Elsevier: San Diego, CA, 1996; p 233.

(32) Ferrari, A. C.; Robertson, J. Raman Spectroscopy of Amorphous, Nanostructured, Diamond-Like Carbon, and Nanodiamond. *Philos. Trans. R. Soc., A* **2004**, *362*, 2477−2512.
(33) Ferrari, A. C.; Robertson, J. Origin of the 1150-cm^{-1} Raman Mode in Nanocrystalline Diamond. *Phys. Rev. B* **2001**, *63*, 121405.
(34) Lefrant, S.; Aldissi, M. The Thermal-Isomerization of Polyacetylene Studied by Raman-Scattering. *J. Phys. (Paris)* **1983**, *44*, 235−239.
(35) Luo, Y.-R. *Comprehensive Handbook of Chemical Bond Energies*; CRC Press: Boca Raton, FL, 2007.
(36) Nagdi, K. *Rubber as an Engineering Material: Guideline for Users*; Carl Hanser: Munich, 1993.
(37) Liu, L.; Ryu, S. M.; Tomasik, M. R.; Stolyarova, E.; Jung, N.; Hybertsen, M. S.; Steigerwald, M. L.; Brus, L. E.; Flynn, G. W. Graphene Oxidation: Thickness-Dependent Etching and Strong Chemical Doping. *Nano Lett.* **2008**, *8*, 1965−1970.